AFRL-VS-TR-1999-1543

Global Ground Tomography

T. Wallace
D. MacEnany
D. Papadopoulos

Advanced Power Technologies, Inc.
1250 24th St, NW Suite 850
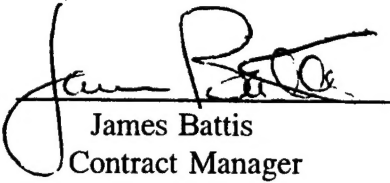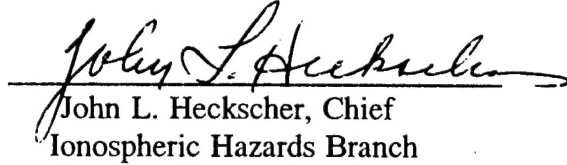Washington, D.C 20037

29 July 1999

Final Report

20000608 114

AIR FORCE RESEARCH LABORATORY
Space Vehicles Directorate
29 Randolph Rd
AIR FORCE MATERIEL COMMAND
Hanscom AFB, MA 01731-3010

DTIC QUALITY INSPECTED 4

This Technical Report has been reviewed and is approved for publication.

James Battis
Contract Manager

John L. Heckscher, Chief
Ionospheric Hazards Branch

REPORT DOCUMENTATION PAGE

Public reporting burden for this collection of information is estimated to average 1 hour per response, including the time for reviewing instructions, searching existing data sources, gathering and maintaining the data needed, and completing and reviewing the collection of information. Send comments regarding this burden estimate or any other aspect of this collection of information, including suggestions for reducing this burden, to Washington Headquarters Services, Directorate for Information Operations and Reports, 1215 Jefferson Davis Highway, Suite 1204, Arlington, VA 22202-4302, and to the Office of Management and Budget, Paperwork Reduction Project (0704-0188), Washington, DC 20503.

1. AGENCY USE ONLY (Leave Blank)	2. REPORT DATE 29 Jul 1999	3. REPORT TYPE AND DATES COVERED Scientific, Final, Oct 1997-Jun 1999	

4. TITLE AND SUBTITLE
Global Ground Tomography

5. FUNDING NUMBERS
F19628-96-C-0145
PE 61102F
PR 4266
TA GH
WW AH

6. AUTHORS
T. Wallace, D. Mac Enany, D. Papadopoulos

7. PERFORMING ORGANIZATION NAME(S) AND ADDRESS(ES)
Advanced Power Technologies, Inc.
1250 24th Street NW, Suite 850
Washington, DC 20037

8. PERFORMING ORGANIZATION REPORT NUMBER

9. SPONSORING / MONITORING AGENCY NAME(S) AND ADDRESS(ES)
Air Force Research Laboratory
29 Randolph Road
Hanscom AFB, MA 01731-3010
Contract Manager: James Battis/VSBI

10. SPONSORING / MONITORING AGENCY REPORT NUMBER
AFRL-VS-TR-1999-1543

11. SUPPLEMENTARY NOTES

12a. DISTRIBUTION / AVAILABILITY STATEMENT
Approved for public release, distribution unlimited

12b. DISTRIBUTION CODE

13. ABSTRACT (Maximum 200 words)
This report describes the work performed during the period 1 October 1997 - 30 June 1999 under the Global Ground Tomography contract, a basic research effort into low frequency electromagnetic techniques for characterization of underground structures.

14. SUBJECT TERMS
Magnetotellurics, Underground imaging

15. NUMBER OF PAGES

16. PRICE CODE

17. SECURITY CLASSIFICATION OF REPORT unclassified	18. SECURITY CLASSIFICATION OF THIS PAGE unclassified	19. SECURITY CLASSIFICATION OF ABSTRACT unclassified	20. LIMITATION OF ABSTRACT UNL

Table of Contents

1. Introduction

This report describes the work performed during the period 1 October 1997 – 30 June 1999 under the Global Ground Tomography contract (contract number F19628-96-C-0145), a basic research effort into low frequency electromagnetic techniques for characterization of underground structures. The current report is the second scientific report produced under this contract; its companion report was issued as Phillips Laboratory Technical Report PL-TR-97-2166.

The major areas of effort during this period were the analysis of data from two blind tests, the conduct of a local source field experiment and an ionospheric source campaign, and analysis of characterization techniques employing vertical magnetic field measurements as an alternative or adjunct to the standard magnetotelluric-type methods employed to date. The work performed in each of these major areas is described in the sections below, followed by a brief summary of conclusions drawn from the entire effort and recommendations for future investigation.

2. Blind Tests

To validate the capability of low frequency electromagnetic techniques to characterize underground structures with unknown locations, this effort included two blind tests. In both cases, data for the blind tests were produced by the U. S. Geological Survey and provided to APTI without information on the number or location of the underground targets present.

2.1. Blind Test 1

The first blind test was performed using data gathered by the U. S. Geological Survey in September of 1997 at the University of Arizona's San Xavier Mining Laboratory south of Tucson, Arizona. The data were provided to APTI in late November 1997, and the results of APTI's analysis were delivered to the Air Force in February 1998.

2.1.1. Data

The U. S. Geological Survey (USGS) collected controlled-source magnetotelluric data using the MT-1 system produced by ElectroMagnetic Instruments. This system collects low-frequency data using natural background noise as a source, and also performs synchronous demodulation of signals from its controlled source at the frequencies given in the table below. The maximum frequency of 25 kHz, as well as the number and spacing of the frequencies collected, are set by the design of the MT-1 system and are not easily modified by the operators.

2

Table 1. Frequencies Used in Blind Test 1

Fundamental	Third Harmonic	Fifth Harmonic
420	1,260	2,100
560	1,680	2,800
890	2,670	4,450
1,190	3,570	5,950
1,320	3,960	6,600
1,610	4,830	8.050
2,500	7,500	12,500
3,290	9,870	16,450
5,680	17,040	
7,350	22,050	
10,900		
14,700		
25,000		

The data consist of remote reference CSAMT measurements taken at 15 stations, numbered 5 to 19, spaced 10 meters apart along a 140 meter line. For stations 8 to 19, the available data consist of AMT (natural noise) measurements for the 79-580 Hz frequency range, and CSAMT measurements at source frequencies from 420-25000 Hz. At stations 5 through 8, only the controlled source data at 420 Hz and above are available. For stations 9 through 11, a second set of data are available, but these measurements were not used in this analysis.

The data were processed beginning with the cross-power files from synchronous detection acquisition. These files were translated into both the format used by APTI's processing, and the EMI standard .RES file format for input to RRI. The data contained in both sets of files were based on exactly the same cross-power input files. To verify that the conversion was performed correctly, the output files were compared with .RES files computed at the time the data were acquired and included in the distributed data.

In some cases, more than one cross-power file existed for the same source frequency. Unless the field notes indicated otherwise, it was assumed that the last file acquired was the highest-quality data, and this file was used when more than one was available. Three

3

of the stations, 11, 13, and 14, had the E_y electrode orientation reversed compared to the remainder of the data. It has not been determined whether the data in the cross-power files has already been corrected for this or not, but this affects primarily the TE mode response, not the TM mode which is of primary interest here.

2.1.2. Target

The data were acquired over the primary tunnel detection target at the San Xavier Mining Laboratory. This tunnel is located beneath station 10 at a depth of approximately 46 meters, and has a diameter of approximately 2 meters, giving a depth to diameter ratio of more than 20. The tunnel has no tracks, pipes, or other conductive objects.

2.1.3. Results of Blind Analysis

The input data were inverted to produce TM mode resistivity estimates using APTI's techniques and RRI; both methods yielded similar results. The results using APTI's algorithm are shown in Figure 1. The estimated horizontal locations given below are expected to be accurate to within one station spacing (10 meters); the estimated depths are strongly dependent on the unknown conductivity of the near-surface region. An unresolved conductive surface layer could cause the estimated depths given below to be too large. Two major features appear in inversions computed with both methods: a resistive feature near the surface located near station 15, and a second deeper resistive feature located near stations 13–16.
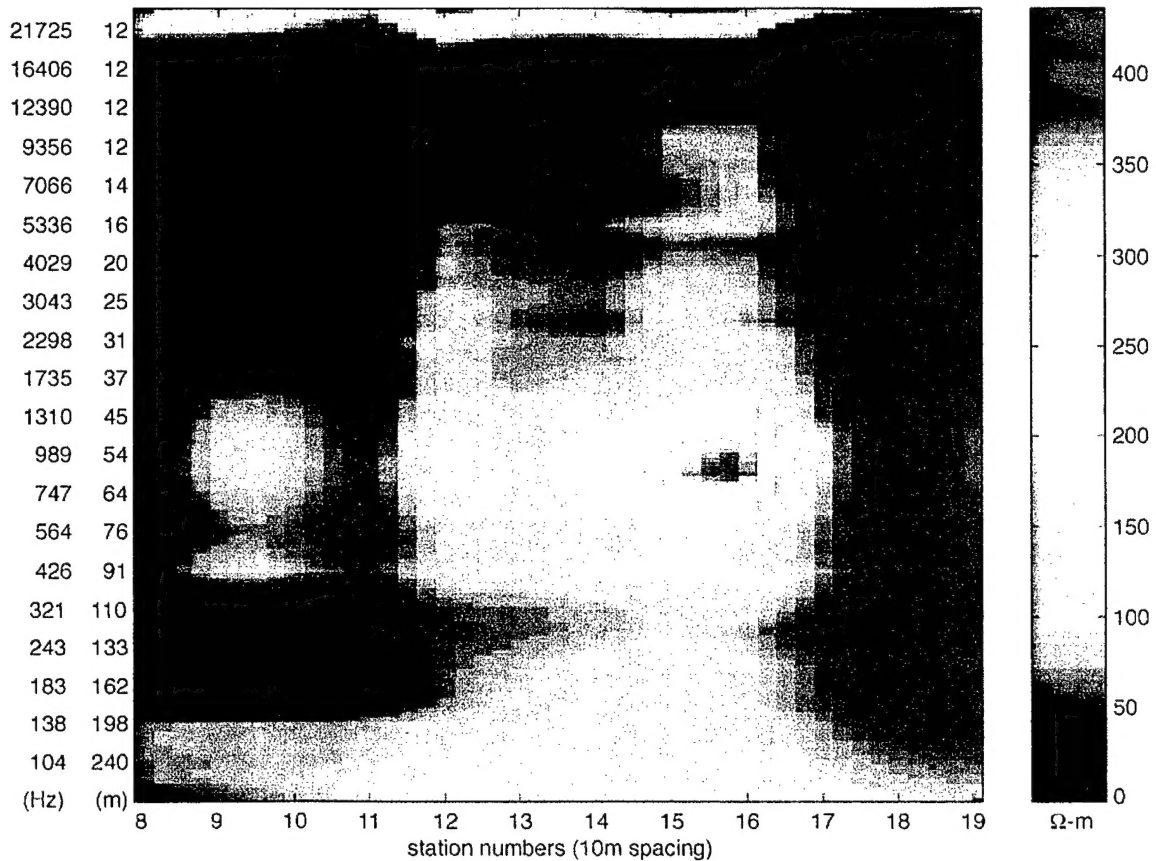
Figure 1. Blind Test 1 Image

The first resistive feature is located near station 15 at an estimated depth of 30 meters or less. The lack of information at frequencies above 25 kHz makes it impossible to determine whether the feature extends up to the surface; examination of the phase data at the highest frequencies provides a slight indication that the feature may not reach the surface. This feature is consistent with a tunnel of diameter 10 meters or less at a depth of 30 meters or less, but would also be consistent with a strongly resistive surface layer; the data are not sufficient to distinguish between these alternatives.

The second resistive feature is located near stations 13–16 at an estimated depth of 50–100 meters. This feature is bounded above and below by more conductive regions, and is consistent with a tunnel of diameter 20–30 meters or less at a depth of 50–100 meters. Some of the inversions show this anomaly as a pair of resistive features, the first near stations 13–14 at a depth of 100–120 meters, and the second near stations 15–16 at a

5

depth of 50–90 meters. It is not clear whether this splitting of the feature into two objects is an inversion artifact, but the inversions clearly indicate the presence of one or more resistive features at this location.

2.1.4. Discussion

Blind analysis of the data did not identify the target. This target was located at a depth to diameter ratio of greater than 20, much deeper than any resistive tunnel has been detected using magnetotelluric techniques. For comparison, the largest depth to diameter ratio at which a restive tunnel is detectable by conventional processing is approximately 3, and the largest ratio at which these targets have been detected by APTI's algorithm is approximately 10. While it is unlikely that the target could have been identified even with extremely high quality data, an additional limitation resulted from constraints imposed by the data collection system.

The MT-1 system collects controlled-source data at only 31 frequencies. Although this is sufficient for conventional processing algorithms, APTI's approach requires information about the smoothness of the response in the frequency domain, and this necessitates obtaining information at more frequencies. APTI's field procedures transmit approximately the same number of source frequencies, but APTI's standard processing is based on the Fast Fourier Transform, rather than the synchronous detection employed by the MT-1. The use of the FFT allows information at many additional frequencies to be obtained by using natural background noise recorded simultaneously with the controlled source. Often, hundreds of additional frequencies are obtained at no additional cost, particularly in the 50–500 Hz and 5–50 kHz bands where background noise is relatively strong. The design of the MT-1 system limits the use of FFT processing to frequencies below 640 Hz, and even then allows only a relatively low resolution. Had the target been located at 20 meters depth, rather than 46 meters, the lack of additional high frequency information might have become the limiting factor preventing detection of the target.

2.2. Blind Test 2

The second blind test was performed using data from simulations provided by the USGS. The data were provided to APTI in August of 1998, and APTI's analysis was returned to the Air Force in early November, 1998.

2.2.1. Data

The data consist of magnetotelluric impedances at 17 stations, spaced 10 meters apart along a 160 meter line. The impedances are given at 25 frequencies from 460 Hz to 46 kHz, as shown in the table below.

Table 2. Frequencies Used in Blind Test 2

460	4,600	46,000
560	5,600	
680	6,800	
820	8,200	
1,000	10,000	
1,200	12,000	
1,500	15,000	
1,800	18,000	
2,200	22,000	
2,600	26,000	
3,200	32,000	
3,800	38,000	

2.2.2. Target

The blind test data set was computed using a two-dimensional forward simulation. Three resistive tunnels, each 5 meters square, were embedded in a layered earth with a slight surface slope. The three targets were located beneath station 4, between stations 8 and 9, and beneath station 12, at depths of 15.4, 43.8, and 35.6 meters, respectively. All three targets were located in the first layer of the model; the second layer began at a depth of 60 meters. The surface slope was gradual, with a total height variation of 3 meters across the profile.

2.2.3. Results of Blind Analysis

The data suggest that the visible features described below are embedded in a one-dimensional background. The 3-layer profile given below produced very good agreement with the data.

Table 3. Estimated Background Resistivity for Blind Test 2

Layer	Thickness	Resistivity
Layer 1	55 m	70 $\Omega \cdot m$
Layer 2	105 m	265 $\Omega \cdot m$
Layer 3	10 m	55 $\Omega \cdot m$
Basement	∞	70 $\Omega \cdot m$

It should be noted that the highest available frequency of 46 kHz yields a skin depth of about 20 meters in a 70 $\Omega \cdot m$ background, making it difficult to determine the depth of targets at shallower depths. It should also be noted that a frequency of 460 Hz is not low enough to sufficiently capture the full signature of the basement resistivity.
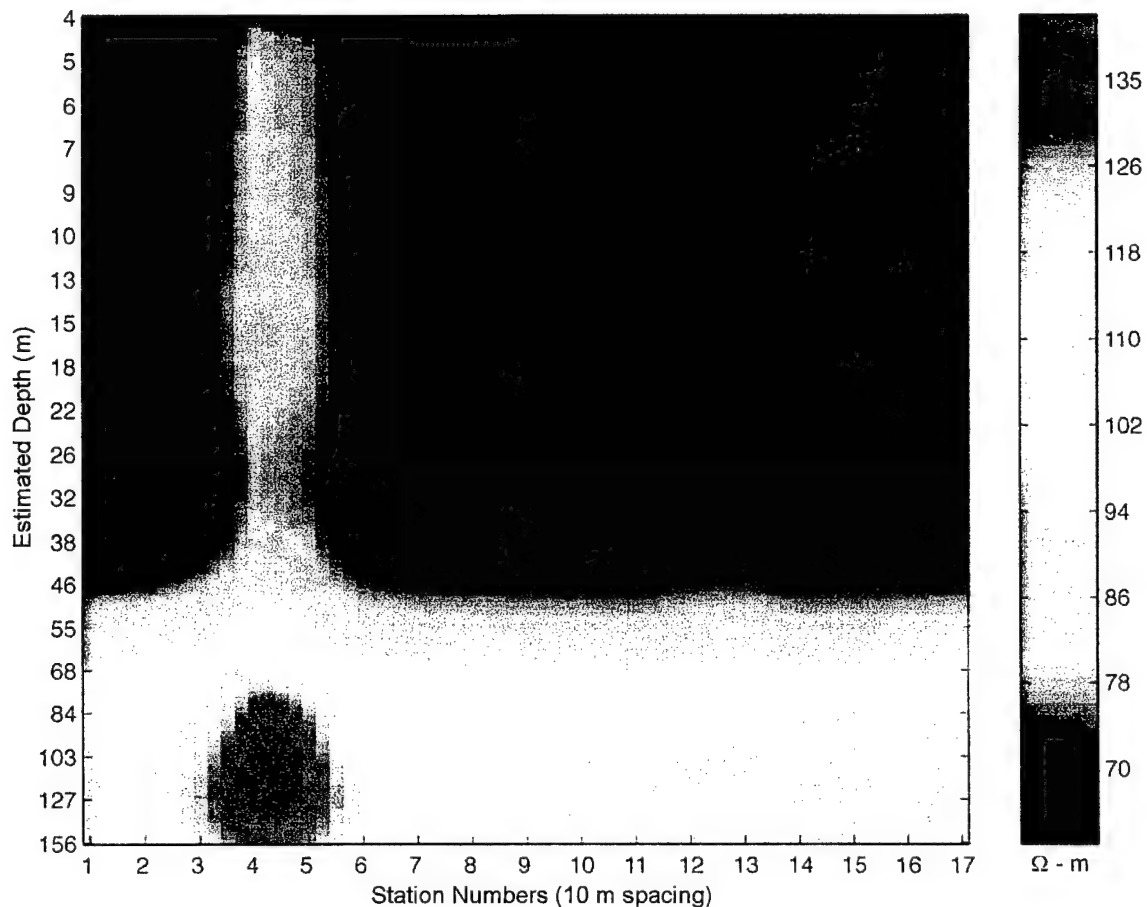
Figure 2. Blind Test 2 Image

The input data were inverted to produce TM and TE mode resistivity estimates using APTI's techniques and RRI; both methods yielded similar results. The results obtained using APTI's algorithm are shown in Figure 2. One major feature and two smaller features are detectable in both TM-mode inversions, although they are more visible in the inversions produced by APTI's algorithm. The estimated horizontal locations given below are expected to be accurate to within one station spacing (10 meters); the estimated depths are strongly dependent on the unknown conductivity of the near surface region. An unresolved conductive surface layer could cause the estimated depths given below to be too large.

The most visible feature is a two-dimensional resistive structure located beneath station 4, with an estimated depth of between 90 and 115 meters. This feature is consistent with a

9

tunnel of diameter 15–25 meters oriented perpendicular to the measurement line, and appears clearly in both the APTI and RRI inversions. It should be mentioned that the second layer of the one-dimensional background, in which this target appears, is more than 3.5 times as resistive as the first layer, and this causes a lag of the current penetration with frequency into the deeper layer. This can lead to difficulties in depth estimation and a reduction of resolution.

The second and third features are much less visible, but appear in the results of both inversions. Both features arise from small perturbations in the input data, and the low density of frequency sampling in the data makes it difficult to determine their depths and, in some cases, even their conductivities precisely.

The second feature is a resistive structure located between stations 12 and 13 at a depth of 100-140 meters; it appears that the structure is either three-dimensional, or a two-dimensional structure not perpendicular to the measurement line. The feature is consistent with a tunnel of diameter 5–15 meters, or a three-dimensional void of diameter 20 meters.

The third feature is a structure located beneath station 4 at a depth of 10–30 meters (that is, located above the larger resistive feature). It appears that the structure is resistive, but the feature appears at or above the upper end of the frequency range of the data, and it is difficult to determine its conductivity or its depth precisely. The feature is consistent with a structure of diameter 1–5 meters.

2.2.4. Discussion

Blind analysis of the data detected two of the three targets present in the simulated data. The estimated depths for these targets were significantly greater than the actual depths, an error which is most likely be attributable to simplifications made in the processing rather than an inherent limitation of APTI's techniques.

Interpretation of the data were complicated by several factors, including one noted earlier in the analysis of the first blind test data set. The data set contained only 25 frequencies,

many fewer than APTI's algorithms typically employ, and fewer even than the first blind test data set. As noted in the blind analysis, the small number of frequencies negatively affected the accuracy of the depth estimates.

A second limitation arose from simplifications made by APTI in the analysis of the data. At the time the data were analyzed, APTI's algorithms treated all conductivity changes as isolated perturbations from a uniform half space. This was the result of choices made earlier in the development of the algorithms to simplify their implementation, and does not represent a fundamental limitation of the approach.

When the actual background has significant vertical conductivity variation, as in this data set, an algorithm based on perturbations from a uniform half space is not directly usable. To process the data, the vertical conductivity variation was first estimated and removed. Then, the remaining conductivity variations were isolated and processed individually under the assumption that they were embedded in a uniform half space. Finally, the resulting targets were reinserted into the vertically varying background. This method can result in significant errors in the estimated target depths, but was necessary because of the characteristics of the input data and the inversions available at the time the data were analyzed.

The optimal approach would have been to process the data using a full two-dimensional inversion incorporating APTI's smoothness constraints. Although APTI is developing such an inversion using internal research and development funds, it was not feasible to complete this inversion in time to use it to process this data. It is expected that this approach would have resulted in depth estimates much closer to the actual depths of the targets.

3. Field Experiments

During the second year of the program, one local source field experiment and one ionospheric source experimental campaign were conducted. The techniques and equipment used were those described in section 4.1 of Scientific Report No. 1 for this effort (Report PL-TR-97-2166), with one significant modification. The manually controlled frequency generator used to provide an input signal to the local source described in section 4.1.1 of that report was replaced by a digital recording played back using a CD player. This eliminated the possibility of operator error in setting frequencies and provided greater flexibility in frequency selection.

3.1. Nevada Test Site Field Experiment

An experiment was conducted at the Nevada Test Site on 30 April–14 May 1998. The target used for this experiment was the Exploratory Studies Facility of the Yucca Mountain Project. This tunnel is a 7.6 meter (25 foot) diameter horizontal shaft approximately 8 kilometers in length, consisting of 3 straight sections forming a C-shaped structure with two portals on the east side of Yucca Mountain (Figure 3). The depth of the tunnel ranges from 20 meters just west of the north portal, to over 200 meters for most of the north-south segment beneath Yucca Mountain.

3.1.1. Experiment Description

Data were acquired at three sites, as shown in Figure 3. The sites were chosen to cover a wide range of target depths. The depths at the three sites were 37.4 meters at site 1 (a depth to diameter ratio of 4.7), 106.5 meters at site 2 (a ratio of 13), and 245.0 meters at site 3 (a ratio of 31). The start of data acquisition was delayed from 4 May until 7 May by delays in the approval process by the Nevada Operations Office of the Department of Energy.
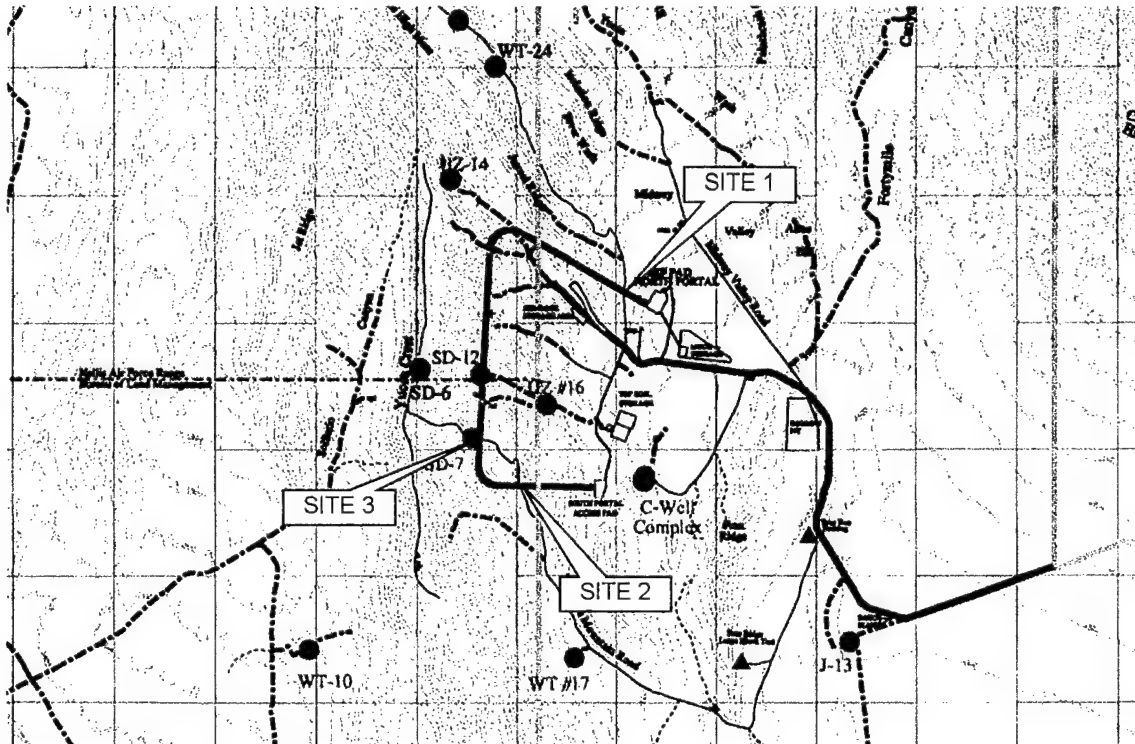
Figure 3. Yucca Mountain Test Locations

Due to an error in positioning, site 1 did not lie over the tunnel as desired. When this error was discovered after the completion of the experiment, each of the 3 sites was resurveyed using differential GPS, which confirmed the error at site 1 and also verified that sites 2 and 3 were located over the tunnel as intended.

During this experiment, the transmitter followed a standard frequency schedule. The normal transmission has a duration of 16 minutes, 58 seconds, and contains the 17 frequencies shown in the table below. The standard frequency schedule and the location and operation times for each site are listed below.

Table 4. Transmitter Frequencies for Nevada Test Site Experiment

Frequency (kHz)	Start Time	End Time
0.8	00:00	00:58
1.0	01:00	01:58
1.2	02:00	02:58
1.5	03:00	03:58
2.0	04:00	04:58
2.8	05:00	05:58
3.2	06:00	06:58
4.2	07:00	07:58
5.0	08:00	08:58
6.4	09:00	09:58
7.5	10:00	10:58
8.0	11:00	11:58
10	12:00	12:58
12	13:00	13:58
15	14:00	14:58
18	15:00	15:58
20	16:00	16:58

At site 1, the transmitter was located on the pad adjacent to Trench 14, west of the north portal. The approximate coordinates of the transmitter were 36° 51' 10" N, 116° 26' 00" W. Data were acquired at 15 stations at this site on 7 May 1998, using a 5 meter station spacing.

At site 2 the transmitter was located on the pad on Yucca Mountain road, immediately north of first tunnel crossing. The approximate coordinates were 36° 49' 50" N, 116° 27' 00" W. Data were acquired at 18 stations at this site on 8 May 1998 using a 7 meter station spacing.

At site 3, the transmitter was located on a pad on Yucca Mountain road, west of the second tunnel crossing. The approximate coordinates were 36° 50' 00" N, 116° 27' 20" W. Data were acquired at 24 stations at this site on 12–13 May 1998 using a 10 meter station spacing.

3.1.2. Results

Because the data at site 1 were gathered at an incorrect location, no attempt was made to process this data. At sites 2 and 3, processing was difficult due to wide variations in the quality of the electric field data. This is believed to be the result of poor ground contact in the very dry soil at the Nevada Test Site. Although an attempt was made to correct for these effects, the residual variation was still quite strong, resulting in vertical banding in the images that was strong enough to mask the signature of the tunnel. Figure 4 shows the results obtained at site 2 (depth estimation was not performed since the target is not visible).
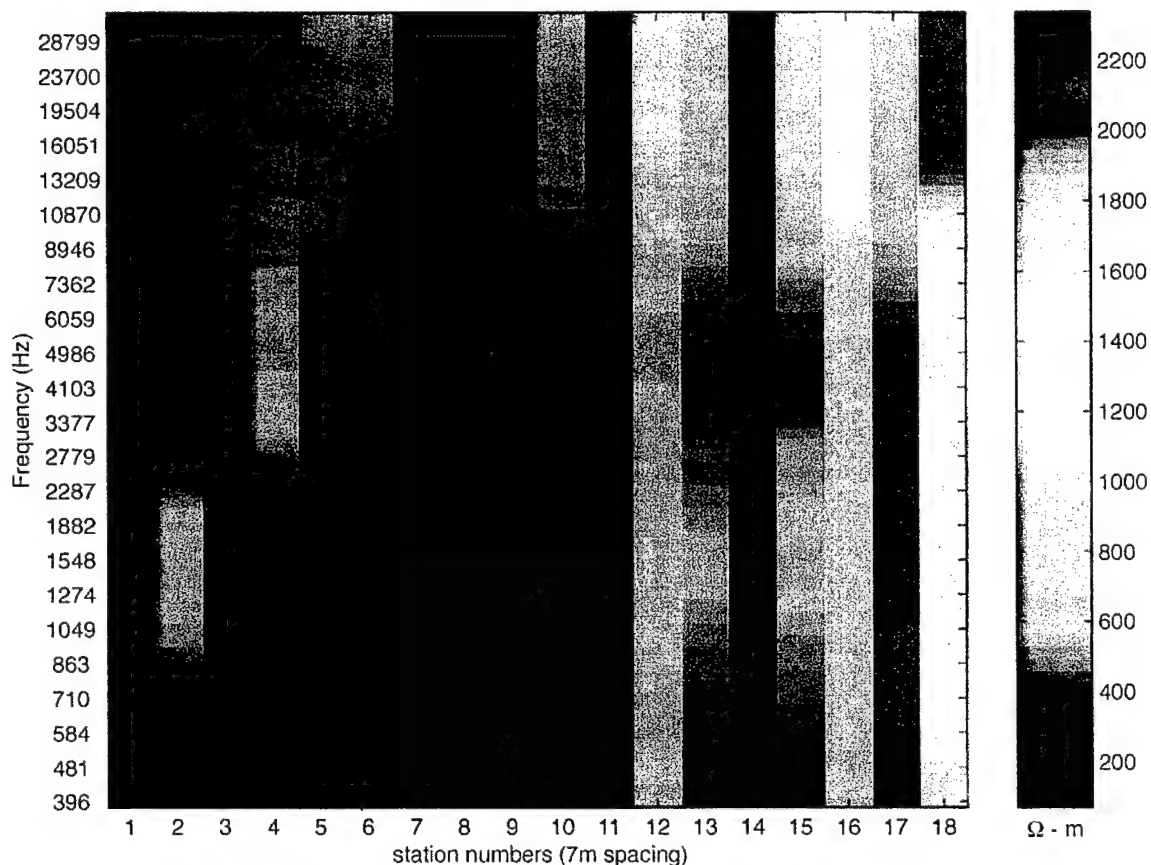

Figure 4. NTS Site 2 Results

The tunnel is located beneath station 9 at a depth to diameter ratio of 13. Although this target might be detectable under ideal conditions, it is obscured here by the vertical banding resulting from poor grounding. Because of the very large depth to diameter ratio

at station 3, and because these data were also similarly affected by poor grounding, data from site 3 were not used to produce an image.

3.2. Silver Fox Ionospheric Source Campaign

An ionospheric source field campaign was conducted 9–20 June, 1998, near Fairbanks, Alaska. The target used was the Silver Fox mine, a small gold and silver mine used for training by the Mining Engineering department of the University of Alaska, Fairbanks. The university allowed unlimited access to the mine site, which greatly facilitated the conduct of the experiment.

3.2.1. Experiment Description

The Silver Fox mine is located 15 kilometers north of downtown Fairbanks. It consists of a single horizontal shaft of diameter 2.5 meters extending approximately 130 meters into the hillside.

The underlying bedrock in this area is granodiorite, and the mine is essentially an unlined tunnel into the bedrock. The gravel access road for the mine crosses over the mine tunnel, providing a convenient location for emplacing sensors; most measurements taken during this campaign were taken with sensors placed on the road.
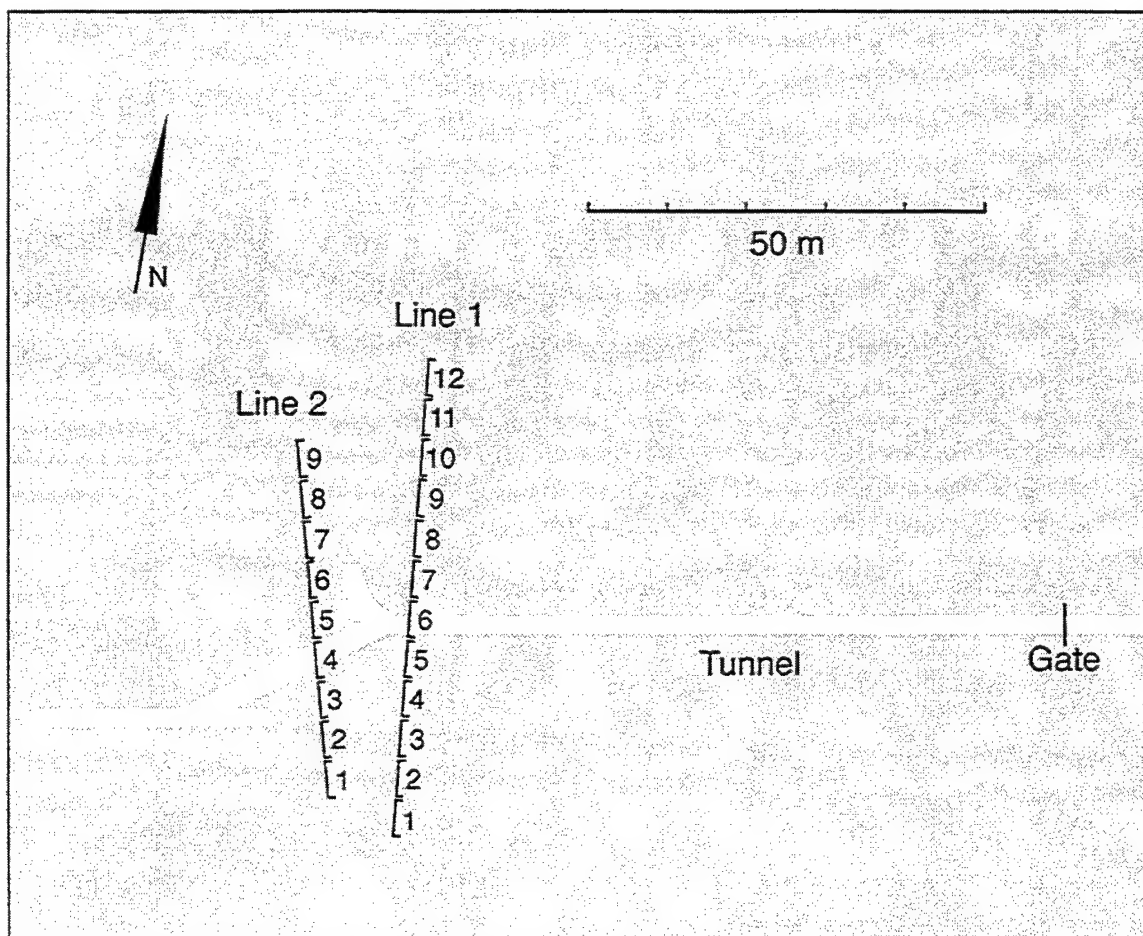
Figure 5. Silver Fox Experiment Plan View.

A plan view of the mine is given in Figure 5. After a 85 meter straight section, the tunnel curves slightly to the left for 25 meters before returning to nearly its original direction for a final 20 meter section. Except for shoring near the entrance, the tunnel is unlined; the only conductors present in the tunnel are a narrow gauge railroad track and a two inch diameter compressed air line, both of which are aligned with the tunnel axis. An interior view of the tunnel is shown in Figure 6.
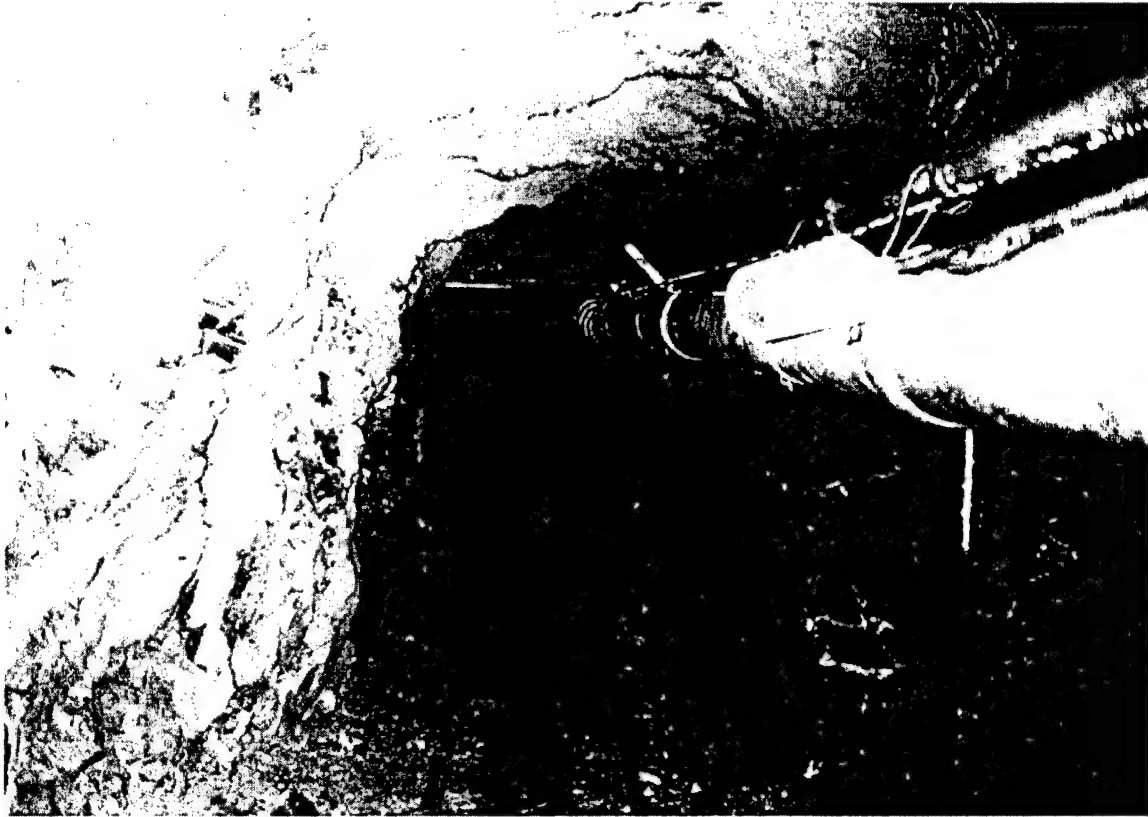
Figure 6. Silver Fox Mine Interior.

The HIPAS facility, used as an ionospheric source for this experiment, is an ionospheric heater operating at 2.85 MHz. It is located east of Fairbanks and is 38.2 kilometers from the target site at a bearing of 113 degrees true (23 degrees south of due east). For this experiment, the HIPAS facility transmitted an X-mode carrier amplitude-modulated at frequencies between 500 Hz and 12 kHz. The facility operated at full power (800 kW), resulting in a magnetic dipole moment under good ionospheric conditions of approximately 5×10^8 amp-m^2. The actual dipole moment obtained varied widely depending on ionospheric activity.

The transmitted signal consisted of a series of frequencies chosen to cover the range of interest for the target site. For each night of operation, a transmission schedule was designed that lasted one hour. On each succeeding hour of operation, the schedule was repeated, to allow data acquisition at another sensor position. The schedule contained a period with no signal at the end of each hour to allow repositioning of the sensors. Two

different transmission schedules were used, one for the standard magnetotelluric data acquisition on 10–12 and 15–17 June 1998, and one for acquisition including vertical magnetic field measurements on 18–19 June 1998. The schedules are shown in the tables below.

Table 5. HIPAS Frequency Schedule for 10–17 June 1998

Frequency (kHz)	Start	End
0.8	00:00	01:30
0.9	01:30	03:00
1.0	03:00	04:30
1.1	04:30	06:00
1.2	06:00	07:30
1.35	07:30	09:00
1.5	09:00	10:30
1.75	10:30	12:00
2.0	12:00	13:30
2.4	13:30	15:00
2.8	15:00	16:30
3.0	16:30	18:00
3.2	18:00	19:30
3.7	19:30	21:00
4.2	21:00	22:30
4.6	22:30	24:00
5.0	24:00	25:30
5.7	25:30	27:00
6.4	27:00	28:30
6.95	28:30	30:00
7.5	30:00	31:30
7.75	31:30	33:00
8.0	33:00	34:30
9.0	34:30	36:00
10.0	36:00	37:30
11.0	37:30	39:00
12.0	39:00	40:30
OFF	40:30	00:00

Table 6. HIPAS Frequency Schedule for 18–19 June 1998

Frequency (kHz)	Start	End
0.8	00:00	01:00
0.9	01:00	02:00
1.0	02:00	03:00
1.1	03:00	04:00
1.2	04:00	05:00
1.35	05:00	06:00
1.5	06:00	07:00
1.75	07:00	08:00
2.0	08:00	09:00
2.4	09:00	10:00
2.8	10:00	11:00
3.0	11:00	12:00
3.2	12:00	13:00
3.7	13:00	14:00
4.2	14:00	15:00
4.6	15:00	16:00
5.0	16:00	17:00
5.7	17:00	18:00
6.4	18:00	19:00
6.95	19:00	20:00
7.5	20:00	21:00
7.75	21:00	22:00
8.0	22:00	23:00
9.0	23:00	24:00
10.0	24:00	25:00
11.0	25:00	26:00
12.0	26:00	27:00
0.1	27:00	28:00
0.2	28:00	29:00
0.4	29:00	30:00
OFF	30:00	00:00

Data were acquired along two lines, as shown in Figure 5. The first line contained 12 stations and crossed the tunnel at station 6 at a depth of 23 meters. The second line contained 9 stations and crossed the tunnel at station 4 (after the bend) at a depth of 24 meters.

3.2.2. Results

This experimental campaign included both the standard measurements using horizontal field data to produce images, and the first attempt to use vertical field data to provide more accurate characterization of conductive structures. The results of the standard measurements are described here; the vertical field results are given in section 4.2 below.

The ionospheric source field levels observed during this experiment ranged from less than the 0.01 pT detection threshold of the equipment to a maximum of 2.1 pT RMS. These levels are significantly lower than those observed in an earlier experiment at the same site using the same ionospheric source, where fields as large as 9.4 pT RMS were observed. In addition, the periods of high field appeared to occur in bursts lasting 10–20 minutes, rather than over long periods, so that only a portion of the data set was acquired during periods of high field. The lower field levels would be expected to reduce the performance of the imaging algorithm by reducing the signal to noise ratio, and the computed images do in fact show lower resolution than those obtained in the earlier experiment.

In an attempt to compensate for the low field levels, composite data sets were assembled from all of the nights of data collection by choosing the periods when the field was highest. These composite data sets were used in all further analysis of the data.
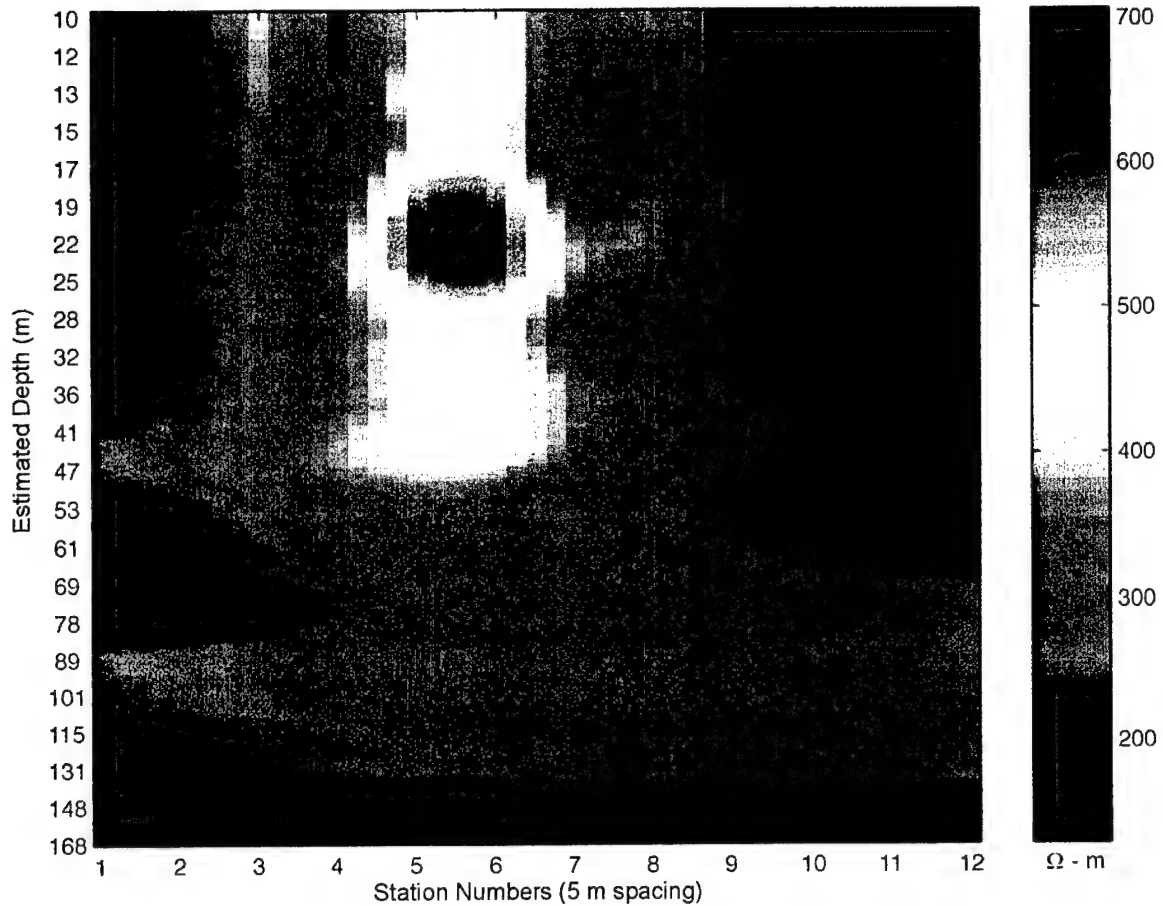
Figure 7. Silver Fox Line 1 Ionospheric Source Results.

A conductivity image produced from ionospheric source measurements along line 1 is shown in Figure 7. The tunnel is located beneath station 6 at a depth of 23 meters, and the known location of the target corresponds well with a resistive anomaly visible in the figure. The 2.5 meter diameter target appears in the image as a region approximately 8 meters across, a factor of 3 reduction in resolution over that observed in an earlier experiment using this target. This reduction in resolution compared to a previous experiment at the same site is believed to be due to the lower signal to noise ratio of the current data.

4. Vertical Magnetic Field Techniques

Because of the practical difficulties associated with obtaining accurate electric field measurements, and because electric field measurements require contact with the ground, it would be beneficial if the standard magnetotelluric technique used to date could be modified to use only magnetic measurements. This would remove a common source of error in data acquisition, and open the possibility of underground imaging from a low flying airborne platform.

As a first step toward the development of such a technique, APTI performed theoretical and computational analyses of the vertical magnetic signatures of buried conductors, and augmented its standard measurements during the Silver Fox ionospheric source campaign described in Section 3.2 above to include measurements of vertical magnetic fields. These results are describe in the following section.

4.1. Theoretical Analysis and Modeling

Conventional magnetotelluric techniques measure the horizontal components of the electric and magnetic fields. By examining the vertical magnetic field component, additional information about the subsurface conductivity may be obtained.

When a plane wave passes over ground with no horizontal variation, the vertical component of the magnetic field (H_z) at or above the surface is zero. The presence of horizontal conductivity changes induces vertical magnetic fields that can be used for characterizing underground targets. This technique can be particularly useful in detecting the presence of conductors in underground facilities, as well as identifying the location of underground conductors.

The vertical magnetic field signature appears when the electric field induced in the ground is parallel to the conductivity discontinuity. In the simplest form, the appearance of the H_z can be understood by considering the 2-D model shown in Figure 8, a vertical

23

contact striking in the y direction at $x = 0$, between uniform quarter spaces with conductivities σ_1 and σ_2, with $\sigma_1 < \sigma_2$.
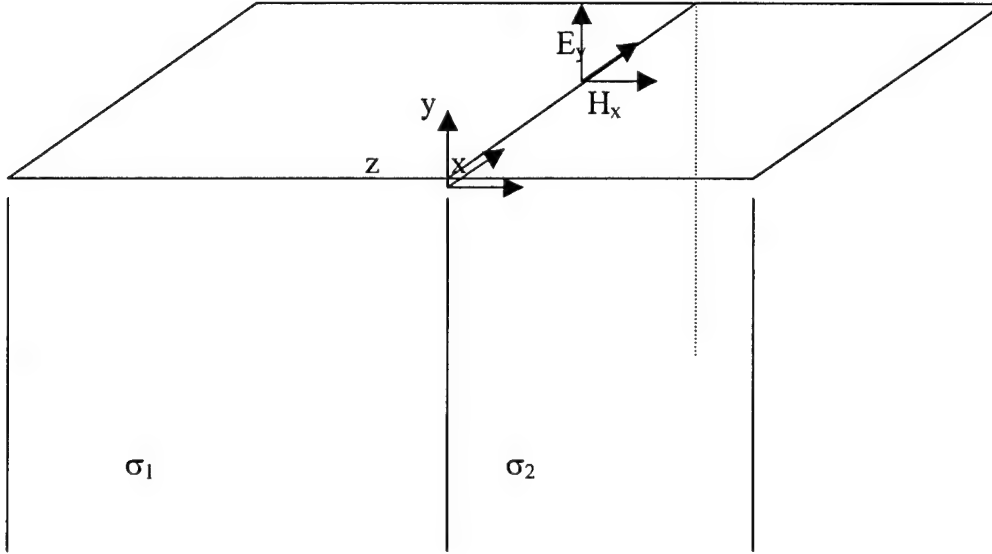

Figure 8. Vertical conductivity contact – E-polarization

The boundary condition requires that **E** be continuous across the boundary and adjust to the skin depth of each side. Currents are squeezed closer to the surface on the conductive side because the skin depth is smaller. Since

$$\nabla \times \mathbf{E} = -\mu \frac{\partial \mathbf{H}}{\partial t},$$

a vertical magnetic field occurs when the curl of **E** has a vertical component. This is equivalent to having a lateral change in the horizontal current. A schematic of the expected response of the normalized vertical magnetic field vs. distance from the discontinuity is shown in Figure 9. H_z exhibits a sharp peak directly over the contact and a relatively rapid decay on either side, falling more slowly on the resistive side than on the conductive side. The peak is caused by the fact that the current density below the resistive side is smaller than below the conductive side causing both the surface and subsurface magnetic field to tilt.
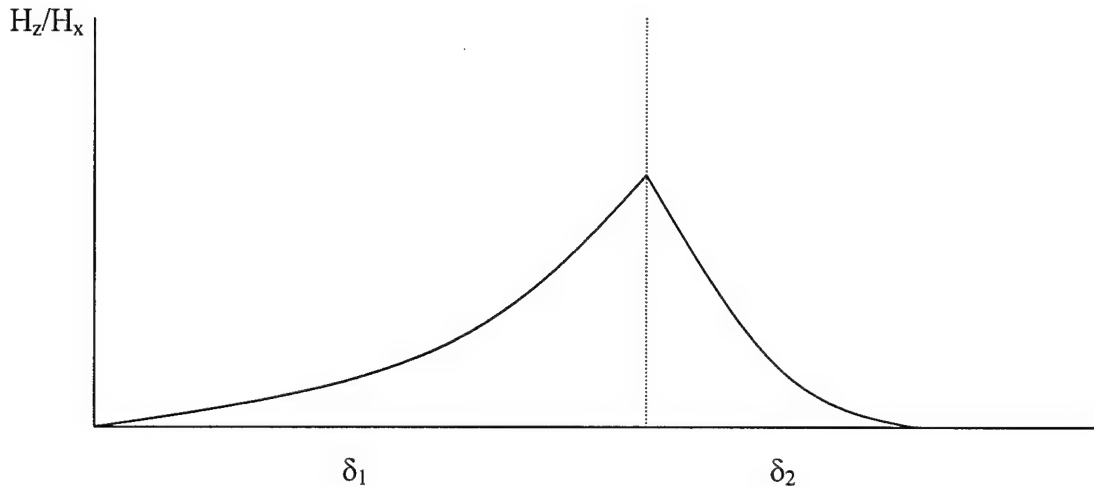
24

Figure 9. Lateral Variation of the Vertical Magnetic Field With Skin Depth

When the conductivity contrast is below the surface, buried beneath an overburden, the effects are smoothed out to a certain extent. The amount of smoothing depends on the thickness and the conductivity of the top layer and on the probing frequency. At high frequencies, when the skin depth is smaller than the thickness of the overburden, the vertical field will be small. Significant vertical fields will appear only for frequencies corresponding to skin depths larger than or equal to the depth of the interface.

The most significant disadvantage of the of the magnetic only measurements is that the information about the value of the conductivity contrast is relativity weak. They can be found implicitly from the decay of H_z with frequency and distance. However, this technique is ideal when the location of the discontinuity rather than the precise value of the conductivity contrast is required. Furthermore, it should be emphasized that quite measurable magnetic field anomalies occur even when both materials are resistive as long as a reasonable conductivity contrast exists.

4.2. Forward Modeling

A number of two-dimensional forward simulations of an underground tunnel with and without conductors, for E-polarization (surface E-field in the y-direction) have been conducted, with emphasis on magnetic-only signatures. The simulations were performed

using the finite element code PW2D, developed by Wannamaker and Stodt and described in Scientific Report No. 1 (PL-TR-97-2166). The results were used as a guide to the conduct of the second Silver Fox experiment, which included a proof-of-principle test of magnetic-only detection, described in section 4.3.

The basic simulation model geometry and parameters is shown in Figure 10. The tunnel with dimensions 2.5×2.5 m is located at a depth of 23 meters in a uniform half-space with conductivity .02 Siemens/m. The conductivity of the tunnel was taken as 10^{-4} Siemens/m. In contrast to the simulations given in Scientific Report No. 1 (PL-TR-97-2166), where the H-mode (surface E-field in the x-direction) was employed, the results below were computed for the E-mode (surface E-field in the y-direction). For all frequencies the incident magnetic field H_x, to which the results should be normalized, was taken as 5×10^{-3}. Two cases are discussed below. In the first case there were no conductors in the tunnel. In the second case two conducting rails were embedded on the ground.

4.2.1. Empty Tunnel

The results of this simulation are shown in Figures 11–13. Figure 11 shows the value of H_x as a function of x for three frequencies (1.5, 1.75, and 2.0 kHz). As expected its value is constant. Figures 12 and 13 show the value of H_z and its phase, respectively, for the above frequencies. The maximum value of H_z/H_x is 4×10^{-4} at a distance of 30 meters about each side of the tunnel and with 180 degrees phase reversal. The decay is consistent with the skin depth, as discussed in section 3.1.1. Whether the H_z signature of the empty tunnel can be measured or not depends on the value of the primary H-field, the planarity of incident wave and integration time.
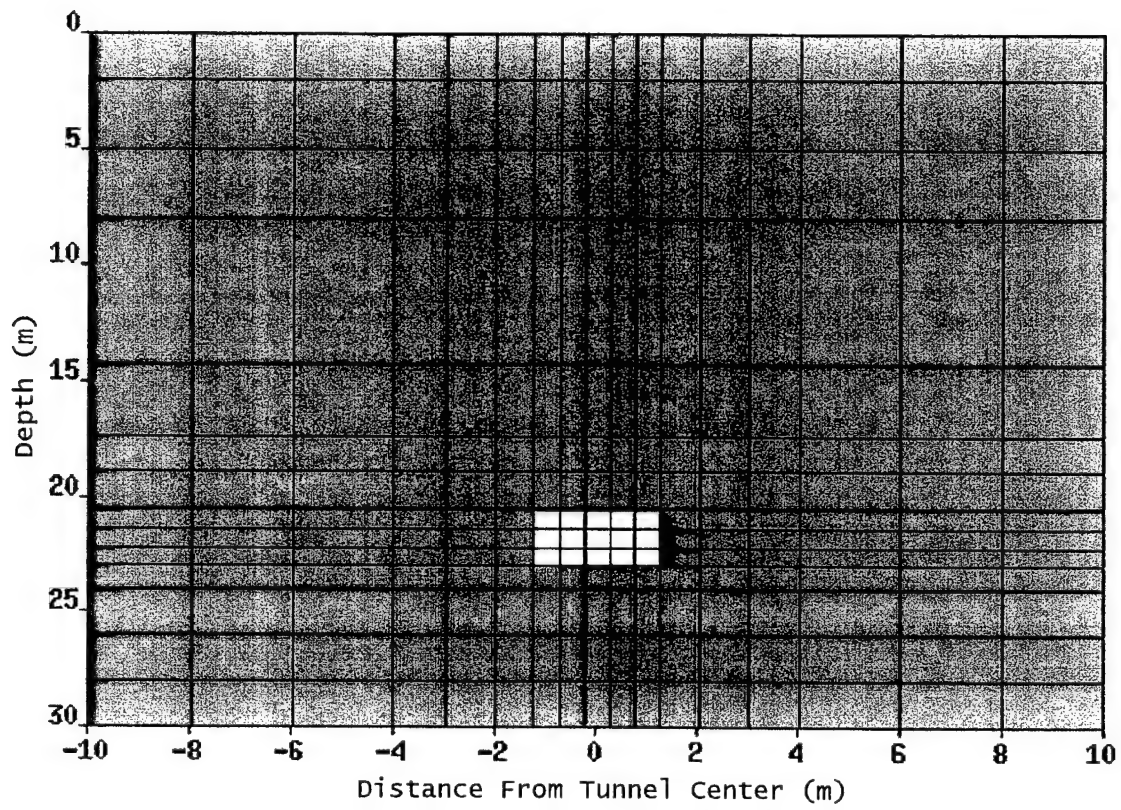
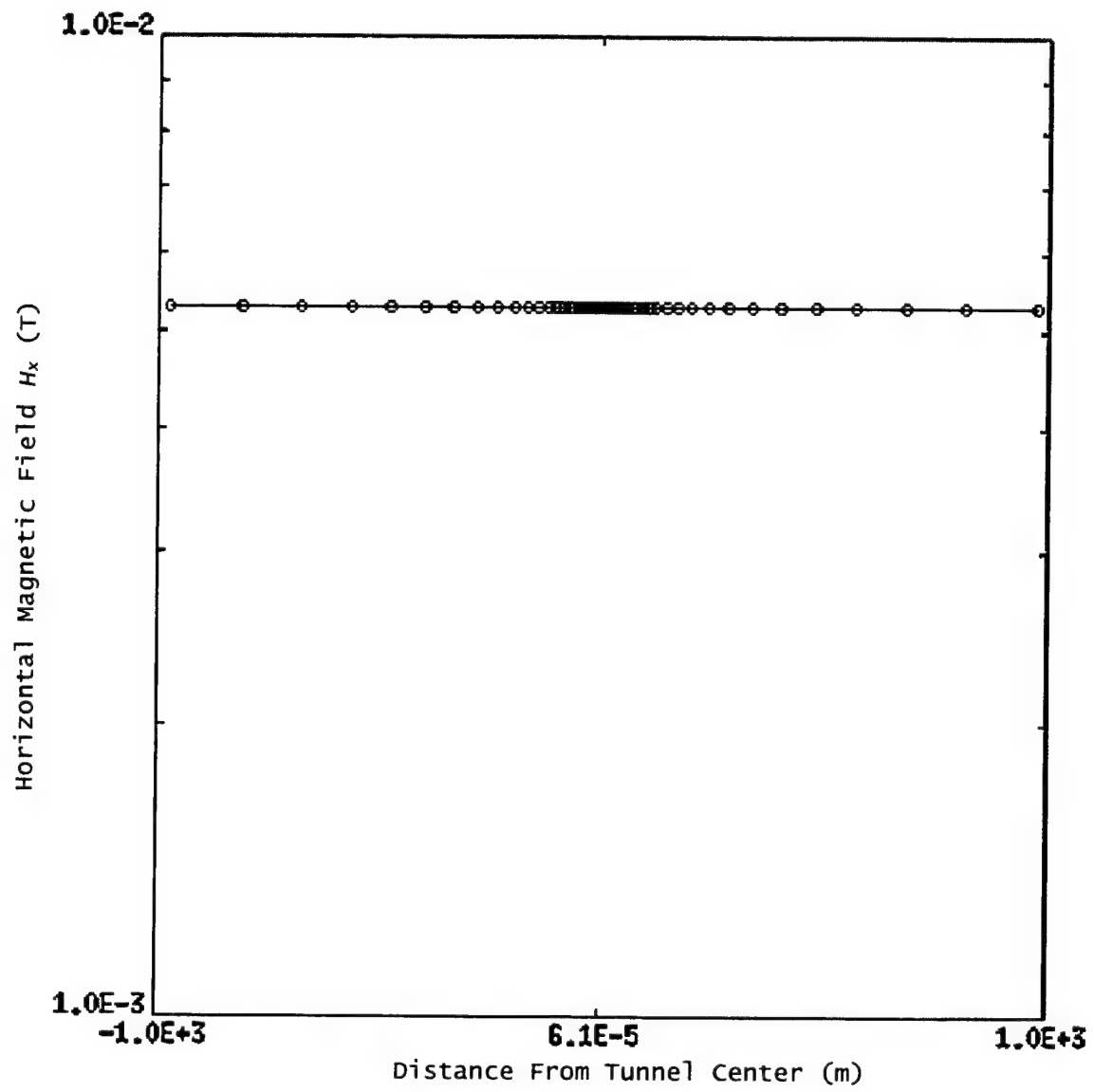Figure 10. Simulation Layout for Empty Tunnel

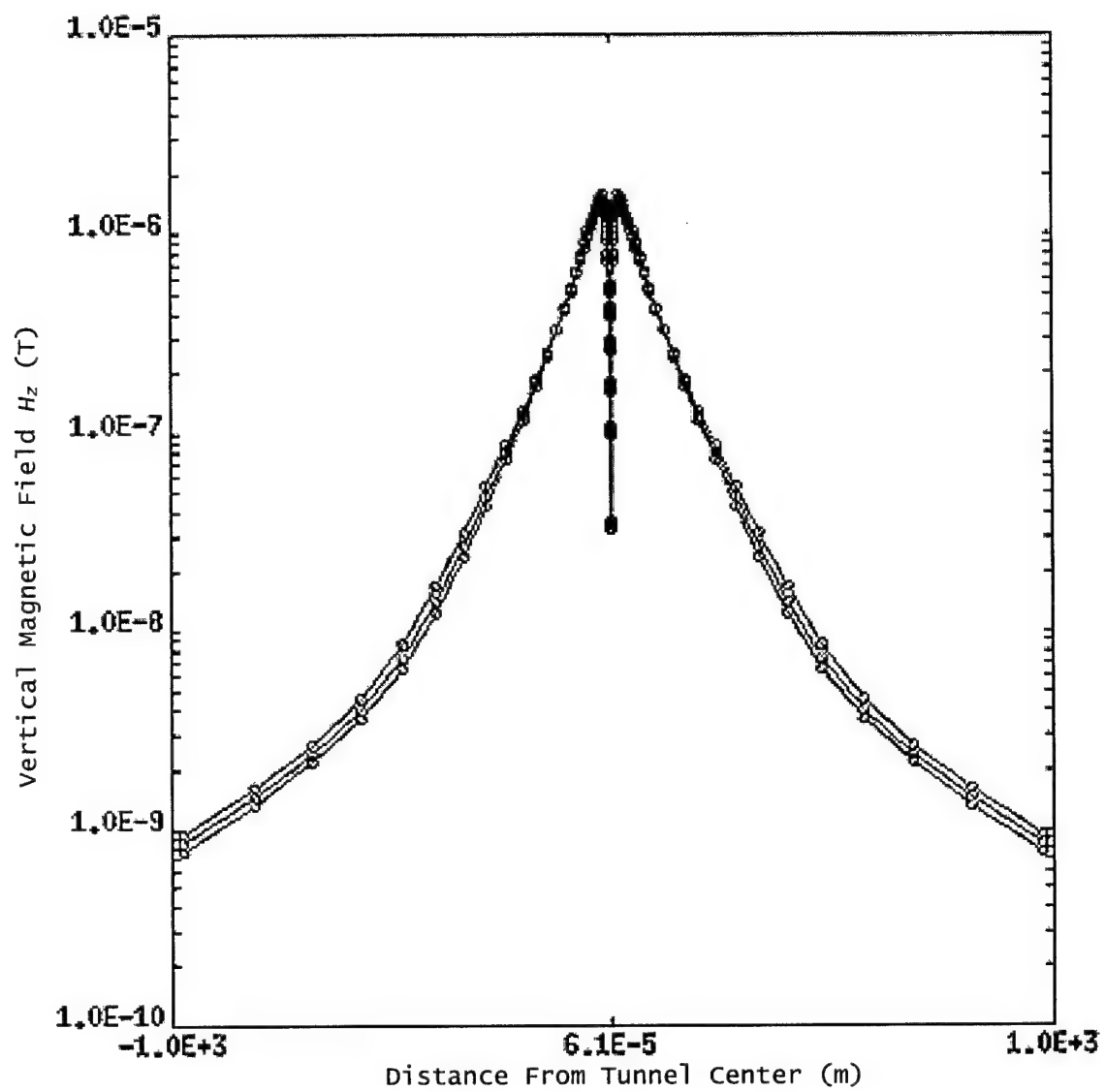Figure 11. Horizontal Magnetic Field for Empty Tunnel
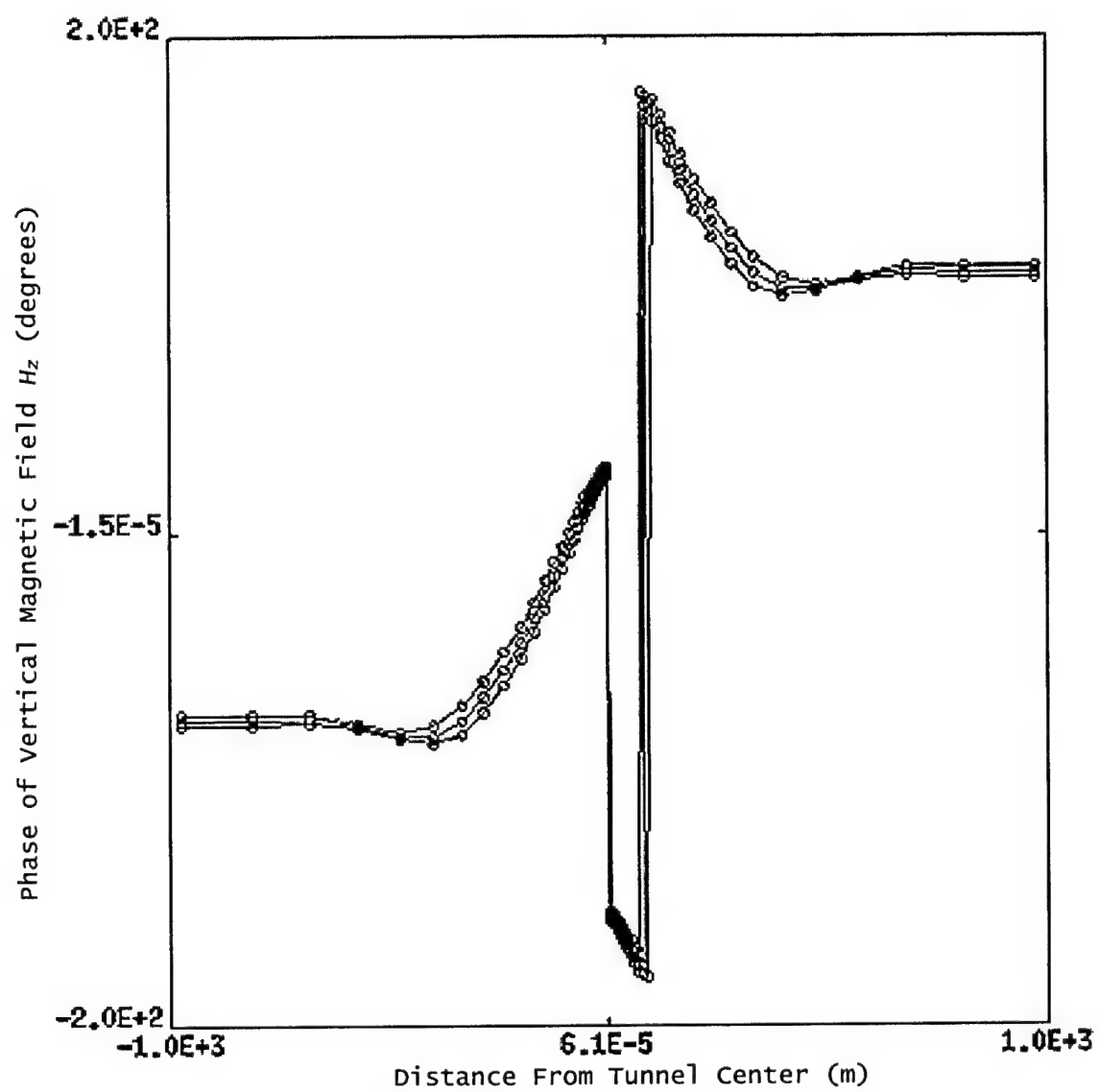
Figure 12. Vertical Magnetic Field for Empty Tunnel

Figure 13. Phase of Vertical Magnetic Field for Empty Tunnel

4.2.2. Tunnel with Rails

The geometry of the next simulation is shown in Figure 14. It is similar to Figure 10 except that two conducting rails with σ =100 Siemens/m have been added, so that the overall configuration is similar to line 1 in the Silver Fox experiment. The results are shown in Figures 15–17. The horizontal magnetic field (Figure 15) shows a perturbation of approximately 20% at distance of about 30 meters on each side of the tunnel. The ratio H_z/H_x has values of about 10% in the same region with opposite phases (Figures 16 and 17). Such signatures are clearly measurable.
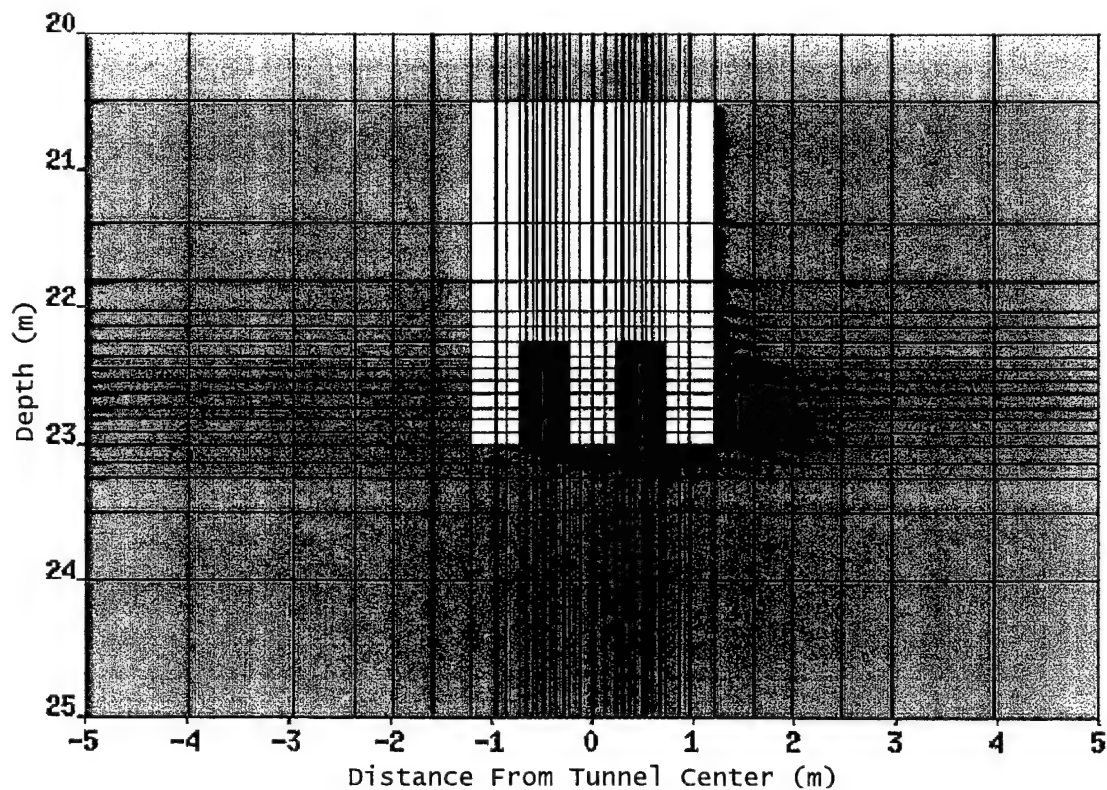

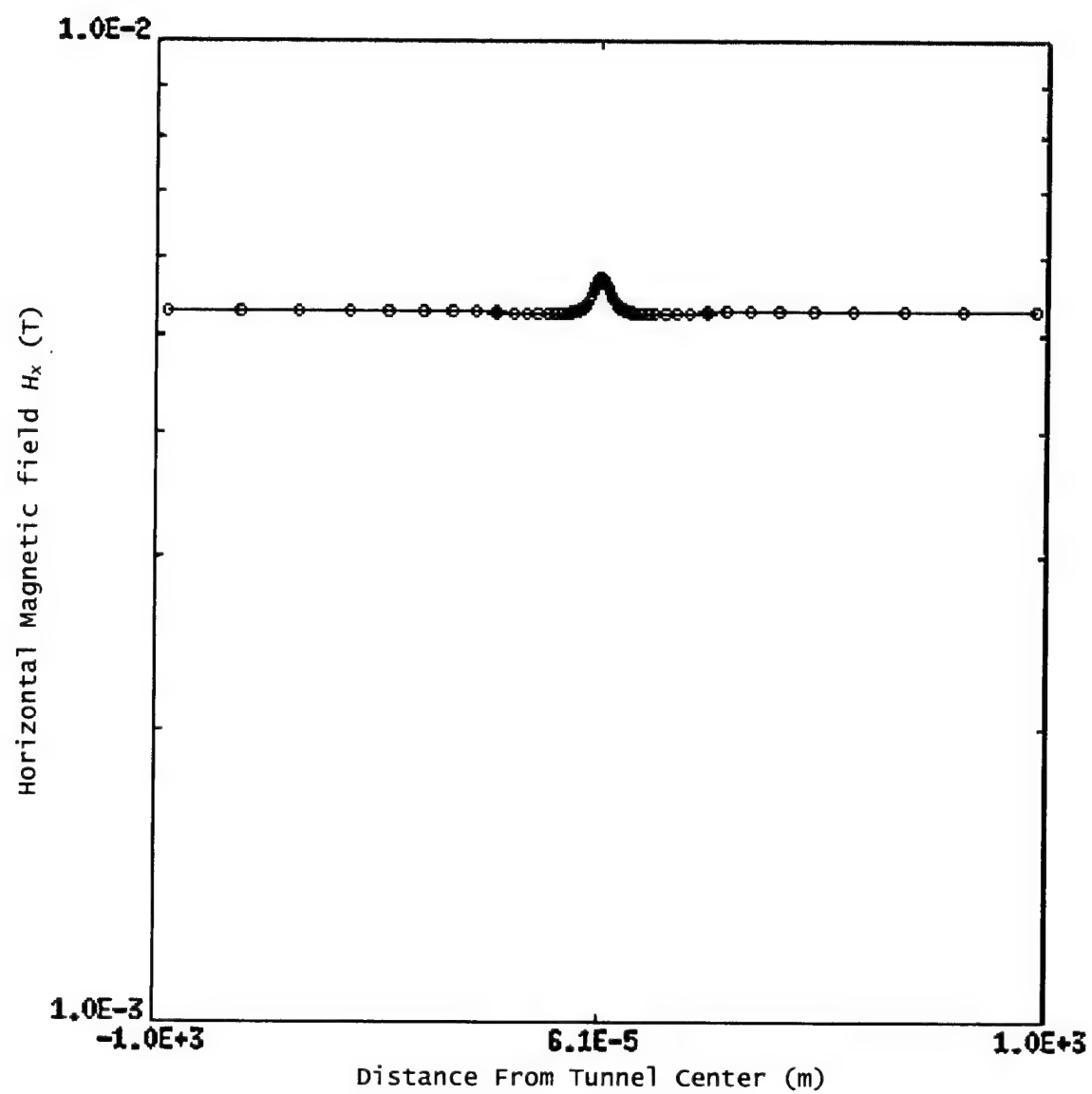Figure 14. Simulation Layout for Tunnel With Rails

31

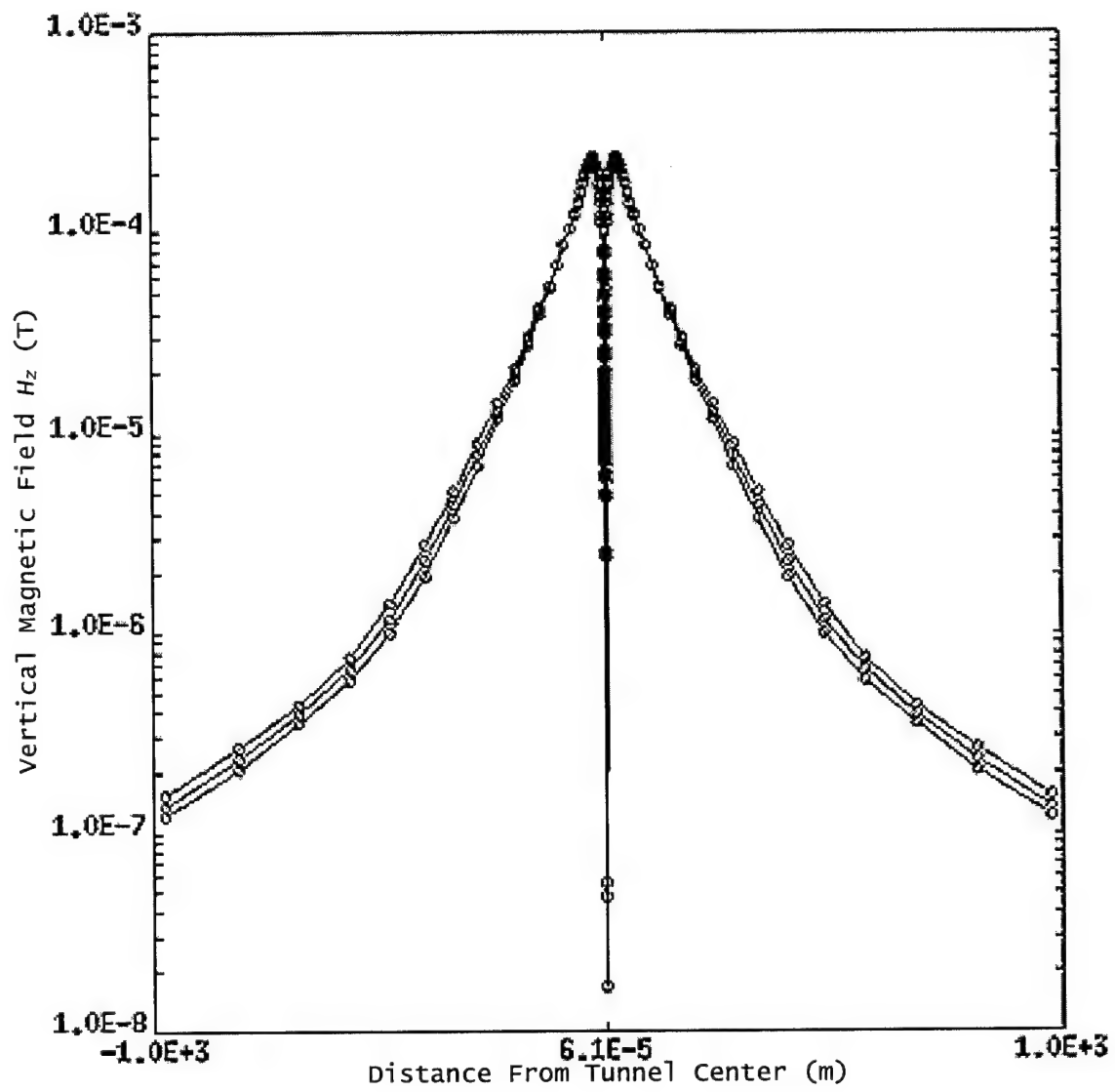Figure 15. Horizontal Magnetic Field for Tunnel With Rails

Figure 16. Vertical Magnetic Field for Tunnel With Rails
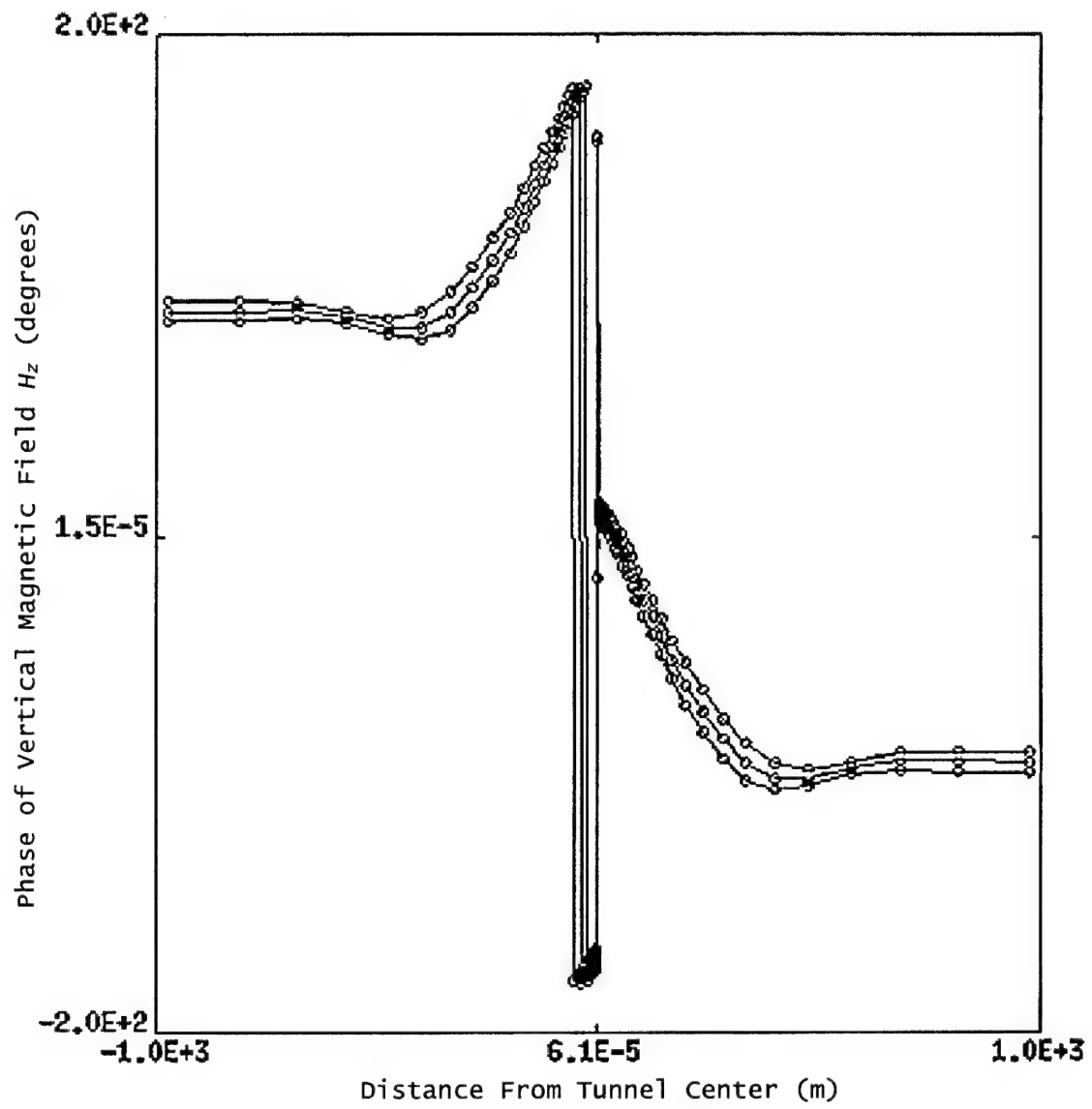
33

Figure 17. Phase of Vertical Magnetic Field for Tunnel With Rails

4.3. Experimental Results

During the Silver Fox mine campaign described in section 3.2, vertical field measurements were made in addition to the usual horizontal measurements. The vertical fields were measured using an additional magnetometer positioned vertically in the center of each measurement station, as shown in Figure 18.

Figure 18. Vertical Field Measurement Setup

Because the incoming ionospheric signal varies rapidly, it is not possible to detect conductors simply by measuring H_z alone. Instead, it is necessary to normalize the measured value of Hz by the value of H_x measured at a location distant from the conductive target in order to remove the effects of the changing source intensity. Here, the x-directed horizontal field R_a measured at the remote reference location approximately 150 meters from the tunnel has been used to normalize the vertical fields.

The measured values of H_z at any given frequency were relatively noisy; to reduce the variation in the ratios, averaging was performed across multiple frequencies. For the 7 transmitted frequencies between 5 and 8 kHz, the ratio $|H_x| / |R_a|$ was computed. Over this narrow frequency range, the ratio should be essentially constant, so each of the 7 ratios should be approximately equal in the absence of noise. The mean and standard deviation

35

of the ratio was computed at each station, and the results of these measurements are shown in Figure 19. The error bars indicate ± 1 standard deviation from the mean.
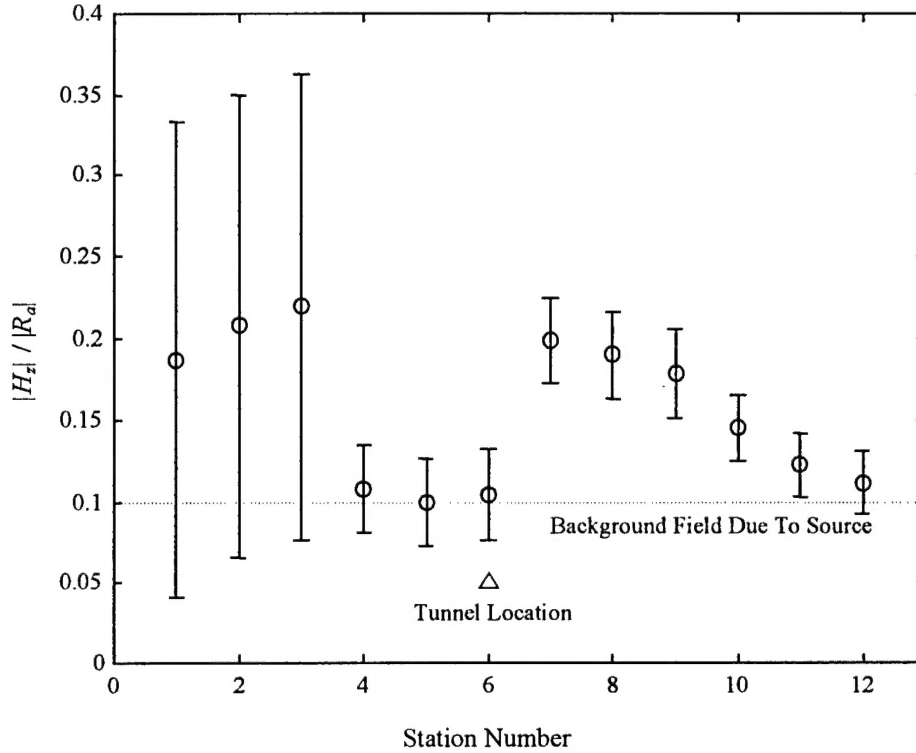

Figure 19. Vertical Field Signature of Silver Fox Tunnel

Although the HIPAS-generated ionospheric source was 40 kilometers horizontally from the measurement site, it was at an altitude of approximately 70 kilometers, and the HIPAS signal appears to have had a significant H_z component even in the absence of subsurface conductors. In no case was a $|H_x|$ / $|R_a|$ ratio of less than 0.1 observed, even at measurement locations far from the tunnel and any other conductors. This background field due to the source would be negligible if the source were located at distance of 100 kilometers or more, since the signal would have fully coupled into the earth-ionosphere waveguide.

The vertical magnetic field signature of the target appears superimposed on this source background field. Consistent with the simulations discussed in the previous section, the additional H_z due to the buried conductors is approximately 10% of the unperturbed H_x.

The observed field ratio signature is not perfectly symmetric, as would be expected if the target was a single tunnel of infinite length. However, as seen in Figure 5, the data were taken at a point near a bend in the tunnel; this departure from the simulated configuration would be expected to produce a broadening of the null and to shift the center of the null in the same direction as the tunnel bend (that is, toward station 1). This is consistent with the data shown in Figure 19.

5. Conclusions and Recommendations

The results documented in this report, and in its companion volume Scientific Report No. 1 (PL-TR-97-2166), demonstrate that low frequency electromagnetic techniques are capable of imaging and characterizing underground targets of military interest. Although much further development is needed to produce a fieldable system, no fundamental limitations have been found which would prevent this, and the remaining practical difficulties are similar in nature to those affecting other techniques for underground structure characterization, such as seismic methods and ground penetrating radars.

It is likely that reliable characterization of underground structures will require fusion of data from multiple sensing techniques, since none of the candidate technologies (electromagnetic, seismic, radar, or hyperspectral) can work reliably over the full range of environments in which hostile underground structures exist. Seismic and low frequency electromagnetic techniques are an attractive complementary pair, since both are capable of imaging deeply buried targets, and since each measures a completely different physical parameter, making simultaneous false alarms much less likely. Continued research and development into low frequency electromagnetic techniques would provide an important addition to other techniques under development.

The potential of techniques employing only magnetic field measurements is significant and has not yet been explored. The results described in this report indicate that these techniques could be especially useful for accurately locating and characterizing buried conductive objects. A particularly attractive feature of magnetic-only techniques is the possibility that they could characterize underground targets from a low flying aircraft or RPV. The potential to characterize a deeply buried target from the air is unique to low frequency magnetic-only methods, and makes further research in this area very attractive.